Metal binding and oligomerization properties of FurC (PerR) from *Anabaena* sp. PCC7120: an additional layer of regulation?

Cristina Sarasa-Buisan, Etienne Emonot, Marta Martínez-Júlvez, Emma Sevilla, Adrián Velázquez-Campoy, Serge Crouzy, M. Teresa Bes, Isabelle Michaud-Soret, María F. Fillat

Journal : **Metallomics. 2022 Oct 20;14(10):mfac077**

DOI: 10.1093/mtomcs/mfac077

Published online: 6 October 2022

Metal binding and oligomerization properties of FurC (PerR) from *Anabaena* sp. PCC7120: an additional layer of regulation?

Cristina Sarasa-Buisan[1], Etienne Emonot[2], Marta Martínez-Júlvez[1], Emma Sevilla[1], Adrián Velázquez-Campoy[1], Serge Crouzy[2] (*in memoriam*), M. Teresa Bes[1], Isabelle Michaud-Soret[2*&] and María F. Fillat[1*&].

[1] Departamento de Bioquímica y Biología Molecular y Celular e Instituto de Biocomputación y Física de Sistemas Complejos (Bifi). Universidad de Zaragoza. 50009-Zaragoza, Spain.

[2] Université Grenoble Alpes, CNRS CEA, IRIG-LCBM 38000 Grenoble, France.

*Both authors contributed equally to this work

[&] Corresponding authors:

MF Fillat fillat@unizar.es

I Michaud-Soret isabelle.michaud-soret@cea.fr

Running title: reversible inactivation of FurC upon oxidation-dependent oligomer formation involving inter-subunit disulfide

Keywords: Ferric uptake regulator FurC, PerR, *Anabaena*, oligomerization, metal binding sites, metal catalyzed oxidation, reversible oxidation.

Abbreviations: FUR: Ferric Uptake Regulator family members; Fur: Ferric uptake regulator protein; P_{prxA}: peroxiredoxin A promoter; ICP-OES: Inductively coupled plasma optical emission spectrometry; RI: refractometry; MALLS: multi angle laser light scattering; MCO: metal catalyzed oxidation, EMSA: electrophoresis mobility shift assays, pLDDT: predicted local distance difference test.

Abstract

Metal and redox homeostasis in cyanobacteria is tightly controlled to preserve the photosynthetic machinery from mismetallation and minimize cell damage. This control is mainly taken by FUR (ferric uptake regulation) proteins. FurC works as the PerR (peroxide response) paralog in *Anabaena* sp. PCC7120. Despite its importance, this regulator remained poorly characterized. Although FurC lacks the typical CXXC motifs present in FUR proteins, it contains a tightly bound zinc per subunit. FurC:Zn stoichiometrically binds zinc and manganese in a second site, being manganese more efficient in the binding of FurC:Zn to its DNA target P_{prxA}. Oligomerization analyses of FurC:Zn evidence the occurrence of different aggregates ranging from dimers to octamers. Notably, intermolecular disulfide bonds are not involved in FurC:Zn dimerization, being the dimer the most reduced form of the protein. Oligomerization of dimers occurs upon oxidation of thiols by H_2O_2 or diamide and can be reversed by DTT. Irreversible inactivation of the regulator occurs by metal catalyzed oxidation promoted by ferrous iron. However, inactivation upon oxidation with H_2O_2 in the absence of iron was reverted by addition of DTT. Comparison of models for FurC:Zn dimers and tetramers obtained using AlphaFold Colab and SWISS-MODEL allowed to infer the residues forming both metal-binding sites and to propose the involvement of Cys86 in reversible tetramer formation. Our results decipher the existence of two levels of inactivation of FurC:Zn of *Anabaena* sp. PCC7120, a reversible one through disulfide-formed FurC:Zn tetramers and the irreversible metal catalyzed oxidation. This additional reversible regulation may be specific of cyanobacteria.

Introduction

FUR (Ferric Uptake Regulator) proteins form a superfamily of pivotal transcriptional regulators present in most prokaryotes. The most ubiquitous members of the family are Fur (ferric uptake regulator), Zur (zinc uptake regulator) and PerR (peroxide response regulator) [1]. In many cases they work not only as metal-concentration dependent regulators, but also respond to different signals, such as the presence of ROS and RNS, O_2, the pH, the ratio C/N or the concentration of NaCl or 2-oxoglutarate [2-7] working as global regulators in a wide variety of bacteria [1]. Despite their common overall structure, different working mechanisms have been proposed for the different FUR regulators, often depending on the number and properties of the metal binding sites, which can vary in the different microorganisms [8]. Furthermore, distinct oligomerization status of some members of the family, such as Fur from *Francisella tularensis* or Zur (FurB) from *Anabaena* (*Nostoc*) sp. PCC7120 (herein *Anabaena* sp.) lead to different ways of interaction of these proteins with DNA [9, 10].

In the nitrogen-fixing cyanobacterium *Anabaena* sp., the *alr0957* gene was identified as the *furC* (*perR*) paralog of the family [11,12]. FurC from *Anabaena* sp. is a 149 amino acid protein containing three cysteines and six histidines. Until now, it was not possible to obtain a fully segregated *furC* deletion mutant of *Anabaena* sp*.,* suggesting a crucial role for that protein in this cyanobacterium. On the contrary, overexpressing FurC produced a viable variant exhibiting a ROS-sensitive, pleiotrophic phenotype with alterations in the photosynthetic machinery and cell-division rate [12]. Indeed, in addition to control a set of genes involved in the response to peroxide stress, FurC (PerR) modulates photosynthesis related genes and is also involved in the regulatory network governing heterocyst development and nitrogen fixation [12, 13].

The function of PerR proteins, which work as metal-dependent peroxide sensors, was first described in *Bacillus subtilis*. Deletion of *perR* led to constitutive catalase expression and overall higher H_2O_2 resistance [14]. PerR from *B. subtilis* (BsPerR) has been further structurally characterized [15] and its action mode deciphered [16]. As purified, PerR is actually a dimer containing one structural Zn^{2+} per subunit bound to four cysteines [15, 17] and one regulatory site per subunit. Upon Fe^{2+} binding in this site, PerR adopts a closed dimer conformation and is able to bind DNA and repress its targets.

In case of oxidative stress, H_2O_2 will react with the regulatory iron, leading to oxidized histidines unable to bind iron anymore and in turn to an open dimer conformation, thus inactivating the protein, allowing for targets de-repression [16, 18, 19]. BsPerR regulatory binding site has high affinity for Fe^{2+} and Mn^{2+} and contains three histidines (37, 91 and 93), being His 37 and His91 sensitive to oxidation mediated by Fe^{2+} and H_2O_2, as well as two aspartates (85 and 104). BsPerR also contains the four characteristic cysteines in the $XH_{91}XH2C_{95}XXC_{98}$ and CXXC motifs (Figure 1). Alternatively, BsPerR has been shown to have also a repressive activity when bound to Mn^{2+} instead of Fe^{2+}, but then is not sensitive to oxidation by H_2O_2 [20] and deactivation by NO [3]. This can be explained by the fact that the oxidation of the histidines is catalyzed in a Fenton like reaction, which Mn^{2+} cannot operate [18].

In *Anabaena* sp., FurC has been shown to be upregulated under H_2O_2 stress conditions, and its DNA binding activity to be metal and oxidation dependent. Indeed, when in a FurC:Zn-Mn situation, FurC has optimal DNA binding activity against *prxA* (peroxiredoxin A) promoter. However, the FurC:Zn-Fe form shows no DNA binding activity without addition of native catalase [11], suggesting that it could work in a similar way to PerR in *B. subtilis* [14,16]. Despite the key role of FurC in cyanobacteria, the presence of the resulting 2-oxo-histidine upon H_2O_2 stress has not been directly demonstrated to date. Likewise, the information about the biochemical properties of FurC, including its metal content, the influence of different effectors in its metalation, oligomerization status and DNA-binding ability is still scarce. In the present work, the metal binding and the presence of oligomeric forms dependent on disulfide bridges was analyzed by SDS-PAGE, both in reducing and oxidizing conditions. On the other hand, size exclusion chromatography combined with light scattering and refractometry (SEC-MALLS-RI) demonstrated the presence of different oligomeric states in solution, such as dimers, tetramers and hexamers. Structural models of these various oligomers were built and analyzed. The metal binding properties of FurC were studied by isothermal calorimetry and ICP-OES. Moreover, FurC metal catalyzed oxidation (MCO) was analyzed through MASS-spectrometry after aerobic incubation of the regulator with Fe^{2+}. Our results suggest two level of response of the FurC sensor to O_2 and H_2O_2, a reversible one involving cysteine oxidation trapping high oligomers unable to bind DNA and the more

classical PerR MCO irreversible oxidation of a histidine in the regulatory site triggering iron release and loss of the DNA binding ability.

Materials and methods

Purification of recombinant FurC:Zn from Anabaena sp.

Pure recombinant FurC:Zn of *Anabaena* sp. was obtained using the procedure previously described [13] with some modifications. Briefly, the *furC* gene (*alr0957*) from *Anabaena* sp. PCC7120 was amplified from *Anabaena* genomic DNA and ligated into pET28a vector (Novagen: Merck, Darmstadt, Germany). FurC:Zn was overproduced in BL21 DE3 *E. coli* cells freshly transformed with pET28a(*furC*) vector grown in Luria–Bertani (LB) medium until the late exponential phase (OD_{600} 0.6-0.7) and induced overnight with 1 mM isopropyl β-D-1-thiogalactopyranoside (IPTG) at 15 °C. 10 g of pelleted cells were resuspended in 50 mL of 50 mM Tris-HCl pH 7.5 in presence of 10 mM EDTA (buffer A) to avoid metal catalyzed oxidation based on the protocol described for the *B. subtilis* PerR orthologue [15]. After lysis by sonication, cell debris was removed by centrifugation, and the resulting supernatant was loaded onto a 20 mL Heparin Sepharose column equilibrated in buffer A. Afterwards, the column was washed with buffer A supplemented with 0.1 M NaCl. Finally, FurC:Zn was eluted in a linear gradient 0-0.5 M NaCl in buffer A. FurC-containing fractions were pooled and dialyzed in 50 mM Tris-HCl pH 7.5. The resultant FurC:Zn was further subjected to an ion exchange chromatography on a 20 mL DEAE cellulose column equilibrated with 50 mM Tris-HCl pH 7.5, washed with 50 mM Tris-HCl pH 7.5, 0.1 M NaCl and separated using a linear gradient of NaCl 0.1 to 0.7 M in 50 mM Tris-HCl pH 7.5. The resulting fractions were analyzed by SDS-PAGE and spectrophotometrically. Furthermore, the tubes containing FurC:Zn were pooled and dialyzed in 50 mM Tris-HCl pH 7.5, 150 mM NaCl to be stored at -80°C. FurC:Zn purification was carried out as well using the same columns but in reverse order performing first DEAE cellulose and heparin sepharose chromatography afterwards, obtaining similar results in oligomer formation, metal content and specific binding activity. For the indicated cases, purified FurC:Zn was further purified by gel filtration on a Superdex 75 HiLoad 16/60 column (GE Healthcare) equilibrated with 50

mM Tris-HCl pH 7.5, 150 mM NaCl and 0.5 mM TCEP. Prior to its injection in the column, FurC:Zn was incubated with 0.5-1 M NaCl during 30 min and with 4 mM DTT during 10 min to favor FurC:Zn dimeric oligomeric state. FurC-Zn quantification was assayed spectrophotometrically using FurC theoretical extinction coefficient at 280 nm (14,440 $M^{-1} \cdot cm^{-1}$).

Metal Content Analysis by ICP-OES

The metal content (Zn and Fe) of purified FurC preparations was determined using ICP-OES at the Servicio de Ionómica from CEBAS-CSIC (Murcia, Spain). All the measurements were recorded in duplicate with 8 to 10 nmol of precipitate-free FurC preparations scaled up to 10 mL of ICP-grade 5 % HNO_3 (Aristar®) (v/v).

MALDI-TOF-MS

The irreversible oxidation of FurC:Zn by incorporation of 1 atom of oxygen per FurC:Zn monomer was elucidated from protein molecular mass determination by MALDI-TOF MS (4800 plus MALDI TOF/TOF, Sciex) performed at the Servicio de Proteómica from Instituto Aragonés de Ciencias de la Salud (Zaragoza, Spain). Prior to the determination, 40 µM FurC:Zn were treated with freshly prepared 40 µM $MnCl_2$ or 40 µM $FeSO_4$ under aerobic conditions for 10 minutes. Afterwards the protein was treated with or without 100 µM H_2O_2 during one hour and then dialyzed for 30 min against Tris-HCl 50 mM pH 7.5, NaCl 150 mM and directly analyzed by MALDI-TOF MS. Briefly, the samples were acidified by adding 0.1 % trifluoroacetic acid (TFA). Samples (0.5 µL) and matrix (0.5 µL of saturated solution of 10 mg/mL of sinapinic acid prepared in 50% ACN/0.1% TFA) were spotted onto an Opti-Tof 384-well insert (Sciex). MALDI-TOF MS analyses were performed in the linear mode with an accelerating voltage of 20 kV, mass range of 25,000–150,000 Da, 1000 shots/spectrum, and laser intensity of 4500. Spectra were externally calibrated using a standard protein mixture (ProteoMass Protein MALDI-MS Calibration Kit MSCAL3, Sigma).

Oligomeric state analysis on gel exclusion chromatography

In order to identify and isolate the different oligomeric states of FurC:Zn a gel filtration on a Superdex 200 Increase column was performed. The column was equilibrated with

50 mM Tris-HCl pH 7.5, 150 mM NaCl. 10% glycerol was added in some experiments as specified in figure legends. Before injection, samples were incubated either without additives, with 2 mM DTT for 10 min or with 0.5 M NaCl for 30 min and 2 mM DTT for 10 min. The isolated species by gel filtration were then analyzed by SEC-MALLS-RI for molecular weight determination.

SEC-MALLS-RI experiments

Multi angle laser light scattering (MALLS) is a technique allowing accessing the precise molecular weight of the species in samples. Knowing that the variation of refractive index related to variation of protein concentration is constant (dn/dC), measuring the refractive index allows one to access the concentration in protein at any point of the elution. Then, thanks to Rayleigh's equation, linking molar mass (M), concentration(C), light scattering (Rθ) which is measured by the captors in the Dawn Heleos-II and an optical constant (K), also calculated by the equipment. The molecular mass of the sample was checked by size-exclusion chromatography coupled to multi-angle laser light scattering with online refractive index (SEC-MALLS-RI) as previously described [21]. 20 µL of sample with a 2 mg/mL^{-1} (122 µM) concentration were loaded on an analytical Superdex-S200 Increase column connected to an in-lane Dawn Heleos II spectrometer (Wyatt Instruments). The column was pre-equilibrated at 0.5 mL.min^{-1} with the buffer, 50 mM Tris-HCl pH 7.5 containing 150 mM NaCl, filtrated at 0.1 µm. 10% glycerol was added in some experiments as specified in figure legends. An in-lane refractive index detector (Optirex, Wyatt Instruments) was used to follow the differential refractive index relative to the solvent. After baseline subtraction of the buffer solution, all samples presented a single peak allowing the determination of absolute molecular masses with the Debye model using ASTRA6 software (Wyatt Instruments) and a theoretical dn/dc value of 0.185 mL·g^{-1}.

Isothermal titration calorimetry (ITC)

FurC:Zn interaction with Mn^{2+} and Zn^{2+} was analyzed with a MicroCal Auto-iTC200 calorimeter (Malvern Panalytical, Malvern, UK) at a constant temperature of 25 °C. Protein solution was used at a final concentration of 20 µM in 50 mM Tris-HCl pH 7.5, NaCl 150 mM. Similarly, ligand solution containing 200 µM $MnCl_2$ or 200 µM $ZnSO_4$ was

prepared in the same buffer as FurC:Zn. A sequence of 2 µL injections (0.5 µL·s^{-1} injection rate) spaced 150 s apart and a stirring speed of 750 r.p.m. was programmed. The dissociation constant was obtained through non-linear least squares regression analysis of the experimental data to a model for a single ligand-binding site for $Mn^{2+}$and Zn^{2+} in FurC:Zn. When indicated, the reducing agents DTT or TCEP at 1 mM and 2 mM respectively and the oxidizing agent H_2O_2 at 500 µM were added to the solutions in order to assess their influence on the FurC:Zn-Mn^{2+} of FurC:Zn-Zn^{2+} interactions. Appropriate controls were performed: Ca^{2+}-EDTA titrations to calibrate/test the calorimeter, and Mn^{2+} and Zn^{2+} dilutions in buffer in order to evaluate the effect of heat associated with the process**.** In order to assess unspecific effects from ligand injection and evaluate the background injection heat effect, control experiments consisting on injecting metal solutions into buffer were performed.

Electrophoretic mobility shift assays

Gel retardation analyses were performed using the promoter region of *prxA* as DNA target and an internal fragment of the *pkn22* gene as nonspecific competitor. DNA fragments of P_{prxA} were obtained by PCR amplification using oligonucleotides 5'-GTCCAGAAGGCGGATTGTC -3' and 5'CTTAATTCTCCTTCAACTTATATCGG3' and then purified using the GFX PCR DNA and Gel Band Purification Kit (GE Healthcare, Buckinghamshire, United Kingdom). A 200 nM protein solution was incubated for 30 min with 50 ng of the corresponding DNA fragments in the reaction buffer containing 10 mM Bis-Tris pH 7.5, 40 mM KCl, 5% glycerol and 0.05 mg/mL bovine serum albumin before being loaded on native 6% polyacrylamide gels. Depending on the tested conditions, 1 mM DTT and/or 0 to 100 µM $MnCl_2$ or $ZnCl_2$ were added to the reaction mixtures.

Determination of intermolecular and intramolecular disulfide bonds

In order to analyze the presence of intermolecular and intramolecular disulfide bonds in the oligomeric species of FurC:Zn, the effects of DTT (Sigma-Aldrich) and H_2O_2 were evaluated. Protein samples at a concentration of 20 µM were treated for 10 minutes at room temperature with 5 mM H_2O_2 and/or with 10 mM DTT. A loading buffer without reducing agents was used. The proteins were resolved by a non-reducing 17% SDS-PAGE and stained with Coomassie blue.

Homology modeling and predictions of oligomeric FurC structures

Homology modelling of FurC dimer was performed using the SWISS-MODEL Workspace (http://swissmodel.expasy.org/). The ab-initio predicted three-dimensional structures of FurC dimer and tetramer were generated using the AlphaFold Colab server [22, 23] that predicts protein structures starting from their sequences using a slightly simplified version of AlphaFold v2.0. This server does not consider existing structural templates. The reliability of the AF predictions was assessed by the Local Distance Difference Test (LDDT) score reported for each structure. The experimental crystallographic structures of PerR and Fur proteins were retrieved from the Protein Data Bank [24] The PISA server [25] was used to assess the oligomeric states of BsPerR which are consistent with its crystal structure (3F8N)**.**

Results

FurC contains a tightly bound zinc per subunit

Sequence alignment of FurC from *Anabaena* sp. with PerR proteins whose crystallographic structures have been solved shows that FurC is devoid of 3 of the 4 cysteines from the canonical CXXC sites which usually coordinate structural zinc in PerR paralogs (Figure 1). Although only the first one (Cys 103) was conserved in the motif, FurC contains two other cysteines in positions 21 and 86 that were not conserved in other PerR homologues. In order to assess the metal content of FurC, ICP-OES analyses were performed using the pool of purified FurC proteins after a two-step procedure consisting in a Heparin Sepharose chromatography, which was carried out in the presence of 10 mM EDTA followed by an ion exchange chromatography on a DEAE cellulose column. Our data show that after purification, FurC keeps 0.83 Zn and 0.31 Fe per subunit (average of two independent measurements as indicated in Supplementary Table S1). This suggests that one Zn^{2+} ion is tightly bound to each FurC protein subunit. Hereafter purified recombinant FurC protein will be referred as FurC:Zn.

Oligomerization analysis of FurC:Zn unveils different types of oligomers

Fur and PerR proteins may exist under different oligomeric states. The oligomerization status of purified FurC:Zn in solution was investigated by size exclusion chromatography (SEC) using a Superdex 200 Increase 10/300 column). Furthermore, a SEC coupled to multi-angle laser light scattering with online refractometer (SEC-MALLS-RI) assessed the molar masses. Figure 2A shows the elution profile of FurC:Zn as purified, incubated under different conditions and afterwards resolved by size-exclusion chromatography. The elution profile reveals several peaks, which correspond to different oligomeric forms of the regulator. It is noticeable that the ratio between peak 1 and peak 2 slightly changes upon addition of DTT, or the presence of DTT plus 0.5 M NaCl, which produces a dramatic increase of fraction 2 (Figure 2A). In order to determine the molecular weights and the degree of oligomerization of the different consortia of FurC:Zn present in these fractions, they were pooled, concentrated and analyzed by SEC-MALLS-RI.

Fraction from "peak 2" contains mainly a dimeric species of 34.9 kDa ± 4.4% (Figure 2E). Identical profiles were obtained in the presence of TCEP reductant in the columns along the whole process (Supplementary Figure S1). It indicates that the reduced FurC remains as a dimer during the previous steps before SEC-MALLS molecular weight determination without reoxidizing into higher oligomeric forms and that intermolecular disulfide bonds are not involved in FurC:Zn dimerization. Fraction from "peak 1" contains a mixture of mainly FurC:Zn tetramers (69.8 kDa ± 12.6%) and dimers (35.6 kDa ± 28.5% kDa) (Figure 2D). The tetramer is the major species in this pool that contains also traces of higher molar masses species. The resulting mixture could be due to an equilibrium between dimer, tetramer and higher oligomers as previously described for *Escherichia coli* Fur [26]. It is noticeable that the dissociation of a fraction of FurC:Zn tetramers and higher oligomeric forms into dimers largely increased in presence of DTT and salt as observed in Figure 2A. In order to have an estimation of the proportion of covalent versus non-covalent interactions between FurC:Zn subunits in solution, a non-reducing SDS-PAGE gel of FurC:Zn as purified before SEC and incubated without and with 10 mM DTT was performed. Figure 2B shows the presence of two major bands around 15 and 30 kDa whose proportion changes depending of the redox conditions. Figure 2C presents a simplified scheme of the most abundant FurC:Zn forms that can be present in solution (left panel) and in the non-reducing SDS-gel (right panel), where non-covalent

interactions are disrupted. The lane containing the sample without DTT in the gel indicates that non-covalent interactions in solution largely contribute to the interaction between FurC:Zn subunits. The disappearance of the upper bands in the sample incubated with DTT suggests the existence of two bridged-subunits in at least one of the species present in FurC:Zn as purified in absence of DTT treatment (Figure 2C). Furthermore, the experiment performed on pure dimer (see below and Figure 3) demonstrates the absence of S-S covalently bridged functional dimers.

Reversible oligomerization upon oxidation and reduction

In order to decipher if the disulfide bridged subunit can be formed upon oxidation of FurC dimer, the impact of H_2O_2 and diamide was checked on purified FurC:Zn dimers and followed by SEC-MALLS-RI (Figure 3A). Before injection, FurC:Zn at 122 µM samples were incubated either without additives, with 5 mM H_2O_2 for 30min, with 5 mM diamide for 30 min, with 5 mM H_2O_2 for 30 min followed by addition of 10 mM DTT for 10 min, or with 5 mM diamide for 30min followed by addition of 10 mM DTT for 10 min. It has to be noticed that adding 10 mM DTT on FurC:Zn dimer did not impact the SEC profile at all (Supplementary Figure S2), whereas adding H_2O_2 or diamide gave the same pattern of profiles with well-defined peaks corresponding to higher oligomeric states that can be seen also on non-reductant SDS-PAGE gel (Figure 3B). Interestingly, DTT addition fully reversed the oligomerization to reform dimeric species (Figure 3A and 3B). Figure 3C presents the molar mass measurement of dimer, tetramer, hexamer and even octamers and higher oligomers after oxidation of the dimer as deduced from Table 1 that compared the theoretical and measured molar mass of possible oligomers. Altogether, an oligomerization occurred upon oxidation of thiols to disulfide bridges by H_2O_2 or diamide, which could be reversed by simple DTT reduction. The reversible oligomerization was not dependent on FurC:Zn concentration as seen at 20 µM of FurC:Zn (Supplementary Figure S2).

Interaction of FurC:Zn with Mn^{2+} and Zn^{2+} : different effects in FurC:Zn activity

In order to explore potential metal-interactions of FurC:Zn at the regulatory site, ITC experiments were carried out in the presence of Mn^{2+} and Zn^{2+} in different redox conditions. Supplementary Figure S3 and Supplementary Table S2 show that FurC:Zn as

purified after Heparin and DEAE columns is able to bind with high affinity ($K_{d\ app} \approx 10^{-7}$ M) around one molar equivalent of Mn^{2+} or Zn^{2+}, with no discernible effect of either DTT, TCEP or H_2O_2. Experimental conditions (i.e. same buffer and the absence of chelators or other competitors) were chosen in order to work in conditions similar to these in EMSA assays. Unfortunately, under these experimental conditions the values obtained for the apparent dissociation constants (Supplementary Table S2) do not permit reliable quantitation of binding affinity (Supplementary Figure S4), since they are just below the lower limit for practical determination of dissociation constants by ITC [27]. Furthermore, it should be taken into account that, at the concentrations used in these assays, proteins with significant affinity for metals ($K_d < 10^7$ M) will be saturated and so a true equilibrium is not present [28].

Since FurC:Zn binds Mn^{2+} and Zn^{2+} with high affinity, we sought to investigate the influence of both metal ions in the DNA-binding activity of the regulator. To test the effects of the presence of these metals, EMSA assays were conducted at different concentration of both metal ions. Figure 4 shows that, *in vitro*, FurC:Zn binds DNA in the presence of both, Mn^{2+} or Zn^{2+}, though the concentration of Mn^{2+} needed for efficient binding to its DNA target P_{prxA} is lower than these of Zn^{2+}. It also shows that the tightly bound zinc is not sufficient for the DNA binding activity on P_{prxA}. Furthermore, the EMSA results demonstrate that the regulatory site of FurC was not previously occupied by the tightly bound Zn.

Evidencing MCO of FurC:Zn promoted by Fe^{2+}

Sequence analysis of FurC shows the presence of the conserved O-donor ligand Asp111 that aligns with Asp104 in the BsPerR sequence (Figure 1). Asp104 is a pivotal residue for the interaction of BsPerR with the regulatory metal and it has been proposed to modulate the sensitivity of this regulator to H_2O_2 [15]. MCO of FurC:Zn was monitored by Matrix-Assisted Laser Desorption/Ionization-Time-Of-Flight (MALDI-TOF MS). Figure 5 shows that, in the presence of Fe^{2+}, the mass of the main peak in the protein profile of FurC:Zn increases 16 Da, even in the absence of other oxidants than O_2, as well as in the presence of H_2O_2 (Figure 5B-5C). However, FurC:Zn oxidation under severe oxidant conditions imposed by peroxide did not take place when Mn^{2+} was present instead of

Fe^{2+} (Figure 5D). Abolishment of DNA-binding activity of FurC:Zn by MCO was confirmed by EMSA assays (Figure 6).

FurC:Zn undergoes a metal independent, reversible inactivation by cysteine oxidation with H_2O_2

Reversibility of FurC:Zn inactivation by H_2O_2 was monitored after preincubation of the regulator in presence and absence of Fe^{2+} prior to EMSA assays. As mentioned previously, MCO promoted by Fe^{2+} under aerobic conditions irreversibly inactivated the protein (Figure 6, lanes 5 and 6) as it was described in other PerR paralogs [15, 20]. Interestingly, FurC:Zn inactivation upon oxidation with H_2O_2 in the absence of iron was reverted by addition of DTT (Figure 6, lanes 4 and 5).

Modelling of FurC unveils metal-binding sites and overall structure of FurC oligomers

In order to better understand the reactivity of FurC and gain novel insights on the biochemical basis of FurC oligomerization, homology models for FurC dimers, tetramers and hexamers were built and compared to ab-initio protein structure predictions using AlphaFold Colab [22]. Figure 7A shows the model obtained for the FurC dimer. Interestingly, though AlphaFold does not consider metals to build the structure, the resulting model corresponds to an active, closed form of FurC:Zn dimer that is thought to be able to bind DNA. Overall, the prediction confidence is very high for each monomer with the exception of N and C-terminals which show low confidence values for the prediction and therefore are depicted as rather disordered structures. Although the confidence score (pLDDT) in the loop comprising ^{86}CDG^{88} sequence decreases to around 87, this value still fits into the 90>pLDDT>70 range which is considered a confident backbone prediction (Figure 7B). Confidence of the relative monomer positions into de dimer can be inferred plotting the Predicted Aligned Error (PAE). According to the lowest PAE values, AlphaFold predicts well-defined relative positions for residues 100 to 150 from each monomer. Therefore, in our dimeric model, the 100-150 sequence preferentially interacts with the equivalent sequence in the other monomer, stabilizing the dimer as already reported in other FurC dimers (Figure 7C). In addition, modelling of the FurC dimer was also performed with SWISS-MODEL using as model templates several PerR proteins with available structures and compared these results with the

AlphaFold FurC prediction (Supplementary Figure S5). Since the best alignment was obtained against *B. subtilis* Mn-PerR (PDB 3F8N), its template was used for further evaluation and comparison with the AlphaFold results (Figure 8A). The analysis of the metal-binding sites when the AlphaFold and the SWISS-PROT models were superimposed (Figure 8B) allowed us to propose that the regulatory metal is likely coordinated by 3 His residues and one Asp, namely His45, His98, His100 and Asp111, in a similar manner than in Mn-BsPerR. However, the fifth residue involved in Mn binding in Mn-BsPerR corresponds to Asp85, which is not conserved in FurC (Figure 1). Instead, Asn93 or Asp96 could be involved in Mn^{2+} coordination by FurC:Zn. However, the Alphafold prediction of the region in FurC containing the residues likely involved in the coordination of zinc, which are located at the C-terminus of the regulator, was predicted with a very low confidence score and showed a much more disordered pattern than in the structure obtained from SWISS-MODEL. Superposition of the Mn-BsPerR structure with the SWISS-MODEL built for FurC (Figure 8C) points to Cys103, Asp105, His144 and Asp147 as plausible ligands for the tightly-bound Zn in the cyanobacterial regulator. It is noticeable that in both, AlphaFold and SWISS-MODEL predictions, Cys86 was located in the highly flexible loop which connects β1 with β2 strands placed at the DNA-binding domain. According to SWISS-MODEL, the distance between the two Cα of the Cys86 inside a dimer unit was 16.3Å, while this distance was around 5.9Å in the predicted dimer using AlphaFold.

Furthermore, in order to get more information about the molecular basis of tetramer stabilization and to visualize the possible disulfide bridges that could be formed under air, we used AlphaFold to predict the structure of tetrameric FurC. Model colored by AlphaFold criteria (Figure 7D) reveals that the overall structure exhibits a fair level of confidence. The lowest values are concentrated in a few residues at both termini, as with the dimer model, as well as in the region of 71 to 100 residues, which are thought to be involved in tetramerization of *P. aeruginosa* FurC [21]. Nevertheless, again, Cys86 was the only cysteine residue whose position in the structure potentially enables it to establish disulfide bonds between FurC subunits (Figure 9). Actually, the distances between Cαs of the closest interdimer cysteines (5Å and 9Å) were shorter than the predicted 16.9Å and 17.1Å distances between cysteines forming a dimer in the tetramer (Figure 9B). Although three of the four distances among Cα of Cys86 residues forming

the tetramer are larger than the 5.9Å measured in the dimer (Figure 9B), since the hinge between the two domains is known to be highly flexible and that there is no hindrance by other residues the formation of an S-S bridge between different combinations, either into a dimer and also interdimer Cys86 upon oxidation could be possible. Interestingly, in contrast to the results obtained for the study with FurC, prediction of a Mn-BsPerR tetramer or higher oligomeric stable assemblies did not envisage. The PISA server predicted only a stable dimer assembly for Mn-BsPerR in solution (AB[ZN]2) with the following stability parameters: 16090 $Å^2$ (surface area); 2927.0 $Å^2$ (buried area); -21.1 kcal/mol (ΔG_{int}) and 17.3 kcal/mol (ΔG_{diss}). Furthermore, prediction of a potential Mn-BsPerR tetramer using AlphaFold and AlphaFold v2 failed as well, due to the presence of interchain clashes in loop residues.

Finally, modelling of the FurC hexamer using AlphaFold v.2 was carried out (Supplementary Figure S6). In average, the resulting hexamer models display pLDDT values >70 with the exceptions of protein N- and C-ends. However, pLDDT values obtained in the buried region of the hexamer which contains the flexible loops comprising Cys86 indicate a low confidence prediction and should be treated with caution.

Discussion

FUR proteins were originally identified as metal-dependent regulators, which worked as classical repressors in a dimeric conformation. However, increasing evidences have demonstrated the multiple chemical sensitivity of these regulators, as well as their essentiality in many bacteria with potential health concern and biotechnological relevance. Furthermore, changes in metal availability and redox status might promote a variety of FUR oligomerization states with different affinities for DNA [4, 29, 30]. Interestingly, unlike members of the family responsible for maintenance of metal homeostasis such as Fur, Zur or Mur, the working mode of PerR is unique in this family since it involves metal-catalyzed oxidation of conserved histidine residues [15, 18]. Previous studies about the function of the *alr0957* (*furC*) gene from *Anabaena* sp.

suggested that its product corresponds to a PerR ortholog [11, 20]. This conclusion was mainly based on the increase of *alr0957* transcription in response to H_2O_2 and the high affinity of FurC:Zn for a set of target genes involved in the management of peroxide stress, such as sulfiredoxin A (*srxA*) and the peroxiredoxins *prxA*, *alr2375* (CGT3), *ahpC* and *alr4404*. However, though the inactivation of FurC:Zn after its incubation in aerobiosis with Fe^{2+}, as assessed by EMSA analysis, points to the MCO of this regulator [20], there were no direct evidences yet showing that loss of FurC activity is due to the formation of 2-oxo-histidine.

In this paper we demonstrate the presence of a tightly bound zinc in FurC, renamed FurC:Zn and the MALDI-TOF analyses (Figure 5) demonstrate the incorporation of one atom of oxygen per monomer of FurC:Zn upon treatment of the regulator with Fe^{2+} under aerobic conditions or after addition of H_2O_2. Conversely, the treatment with Mn^{2+} plus H_2O_2 did not produced oxo-FurC:Zn. This oxygen incorporation leads to irreversible inactivation of FurC:Zn, as seen in EMSA, that could not be reversed by DTT (Figure 6). These results, together with the presence in the sequence of the histidine counterparts which result oxidized by MCO in BsPerR [15] (Figure 1), strongly suggest that FurC:Zn undergoes MCO. The ability of FurC:Zn to bind a second Zn^{2+} ion raises the possibility that not only Mn^{2+}, but also Zn^{2+} could protect FurC:Zn from MCO, which only would take place when the relative availabilities of Fe^{2+} versus Mn^{2+}/Zn^{2+} reach a threshold value, as is the case of BsPerR [16].

SEC-MALLS-RI oligomerization analysis under different conditions evidence that FurC:Zn in its most reduced conformation is a dimer. Therefore, dimerization of FurC:Zn occurs without the participation of disulfide bonds. However, this technique preserves FurC:Zn-FurC:Zn interactions not involving disulfide bridges, such as electrostatic interactions. Conversely, non-reducing SDS-PAGE breakups non-covalent interactions in solution, allowing detection of intersubunit disulfide bridges. On the other hand, the SEC-MALLS-RI results showed that a clear transition between FurC:Zn tetramers, hexamers and octamers to the dimeric form occurs in the presence of DTT. Hence, integration of SEC-MALLS-RI and non-reducing SDS-PAGE studies show that both, disulfide bonds and non covalent interactions participate in FurC:Zn-FurC:Zn interactions and the oligomeric status of FurC:Zn. Furthermore, the inactivation of the protein by H_2O_2 regardless of the

presence of Mn^{2+} was easily reverted by DTT treatment, as observed in EMSA assays. These results suggest that the redox status of FurC:Zn cysteines might be important to modulate the activity of this regulator. Likewise, the analysis of the Superdex profile of FurC:Zn as purified, coupled to DTT treatment on the non-reducing SDS PAGE is in accordance with the oxidation of thiol bridging two FurC:Zn subunits together (Figure 2). Furthermore, the SEC-MALLS RI data coupled to non-reducing SDS PAGE experiments (Figure 3) starting from pure dimeric FurC:Zn treated with H_2O_2 or diamide and followed by DTT reduction, decipher the impact of reversible cysteine oxidation on the oligomeric states of FurC:Zn. Therefore, these results show that FurC:Zn dimers do not contain disulfide bridges between the two subunits in the dimer, while the higher oligomeric states characterized: tetramer, hexamer, octamer and higher (Figure 3 and Table1) present disulfide bridges. Indeed, DTT treatment triggers the complete transformation of the protein into dimers that did not contain disulfide bridges anymore.

It is remarkable that, with the exception of the *Leptospira interrogans* regulator [31], which only contains one cysteine residue and is devoid of structural zinc, all PerR proteins whose structures are available to date exhibit only four cysteine residues. These four cysteines are arranged in the two canonical CXXC motifs which likely are coordinating the structural zinc [1, 6, 17, 31]. Therefore, under mild stress conditions zinc-bound thiolates are maintained in its reduced state and are not available to perform thiol-disulfide exchanges. The ICP-OES results indicated that though FurC lacks the canonical CXXC motifs, each FurC monomer contains one tightly bound Zn ion even after purification in the presence of EDTA (FurC:Zn) (Supplementary Table S1). This result was confirmed either with a pool of purified FurC:Zn which contained dimers, tetramers as well as a minor fraction of higher molecular weight aggregates. The ratio of one zinc ion per FurC:Zn subunit was observed as well when the fraction containing the dimeric form of the regulator was isolated from this pool by gel filtration (Supplementary Table S1). This result suggests that zinc is participating in the stabilization of intermolecular interactions between FurC:Zn subunits in the dimer [8, 32, 33]. Additionally, according to ITC analyses, under aerobic conditions FurC:Zn is able to bind either Mn^{2+} or Zn^{2+} in a ratio (1:1) with high affinity. Interestingly, binding affinity of both metals was independent of the redox status of FurC:Zn, suggesting that the cysteines involved in the disulfide bridges present under non-reducing conditions are not coordinating Mn^{2+}/Zn^{2+}

metals at the regulatory site. Furthermore, since DTT and TCEP do not affect FurC:Zn affinity for Zn^{2+} nor for Mn^{2+}, it could be hypothesized that the oligomerization step due to cysteine thiol oxidation does not impact FurC:Zn metal content and, therefore, nor the regulatory neither the zinc sites would undergo important alterations in their close environments.

In good concordance with the ICP and ITC analyses, the modelling of FurC dimers suggests the presence of two potential metal-binding sites per monomer. The folding of the FurC model built using BsPerR as template points to Cys103, Asp105, His144 and Asp147 as the residues forming the Zn^{2+}-binding site. Metal at the regulatory site would be likely coordinated by His45, His98, His100 and Asp111, which are conserved compared to BsPerR. The fifth ligand in BsPerR, namely Asp85, is not present in the sequence of FurC. Instead, Asn93 or Asp96 could be involved in the coordination of the regulatory metal. Modelling of FurC dimers and tetramers also shed some light on the structural features of the regulator and the potential role of FurC cysteines in its reversible oxidation. The models point out the Cys 86 as the one involved in the disulfide bridges between to subunits of the two different dimers in the tetramers. The reduction of this Cys86 may cause a repulsion of the two dimers disfavoring the dimer-tetramer equilibrium in favor of the dimer in reductive conditions and in favor of the tetramer in oxidative conditions clipping the two tetramers together through the disulfide bridge formation. In this way, a regulation could take place since the repressor would be released from DNA upon MCO oxidation and the free repressor pool can be trapped in oligomers which could not be activated by metal for DNA binding until the redox environment of the cytosol came back to normal; this independently of the metal status in the cell.

An oxidative dependent oligomer formation has been already described in other members of the FUR family, such as FurS from *Streptomyces coeliocor* with a redox tetramer stabilization [34, 35], and in *H. pylori* Fur where a Cys78 mutant was produced to avoid redox dependent oligomer formation [32, 33] and even in BsPerR [14] where H_2O_2 treatments trigger oligomer, dimer and monomer formation. In *E. coli* Fur, tetramer and oligomer formations, not involving disulfide bridge formation, were observed in low salt, low pH and high concentration conditions with a high K_d value in

favor of the dimer [26]. On the contrary, highly stable tetramers without disulfide bridges were described for the Fur regulators of *P. aeruginosa* and *F. tularensis* [21]. Furthermore, a reversible oxidation of *Streptococcus oligofermentans* PerR mediated by cysteines has been reported [36]. However, this mechanism differs from the reaction observed with FurC:Zn, since the oxidation in *S. oligofermentans* PerR takes place between two of the cysteines coordinating the Zn^{2+} ion ($C_{139}XXC_{142}$), while FurC:Zn contains a single cysteine (Cys103) in the tightly-bound Zn^{2+} site. Furthermore, since disulfide-bound tetramers contain one Zn per monomer of FurC, it can be concluded that Cys103 is not involved in FurC:Zn reversible oxidation triggering oligomer formation.

Intriguingly, the Cys86 was not conserved into the Fur and PerR members of the family. However, a comprehensive alignment of FurC orthologs annotated in the available cyanobacterial genomes [37] shows that Cys86 is a highly conserved residue in FurC proteins from nitrogen-fixing, heterocystous cyanobacteria (Supplementary Figure S7). It could be speculated that the dual oxidation of FurC may be an optimization of this regulator related to the different redox conditions of heterocysts and vegetative *Anabaena* cells. Both, the photosynthetic machinery and the nitrogenase complex impose a high demand for metals and may deliver electrons to adventitious acceptors resulting in the generation of ROS. However, O_2 evolution occurs only in vegetative cells and changes depending of the light conditions, whereas heterocysts are microoxic since nitrogenase is O_2 sensitive [38]. A clear link has been established between PerR and aerotolerance in anaerobes. In the strict anaerobe *Clostridium acetobutylicum* PerR acts as a switch for oxygen tolerance [39], while PerR:Zn,Fe can also be oxidized by oxygen leading to inactivation of the regulator [5]. Therefore, the activity of FurC:Zn could be differentially regulated in vegetative cells and heterocyst, though further *in vivo* assays are required to evaluate this hypothesis.

Overall, our results show a new *in vitro* regulatory mechanism for a PerR paralog and provide compelling evidence that FurC:Zn undergoes two levels of oxidation as result of both, the redox status of the cell and metal availability, as summarized in Figure 10. Under mild oxidant conditions and iron deficiency dimers of FurC:Zn are reversibly oxidized, likely through inter-dimer disulfide bridges between Cys86. It traps the free

FurC pool from metal activated DNA binding. This type of oxidation could also occur at moderate iron availability but excess of Mn^{2+} (high Mn^{2+}/Fe^{2+} ratio), not shown in Figure 10 for clarity. In this way, FurC:Zn would not be available for DNA binding, though activity of the regulator can be quickly recovered when conditions become favorable, such as iron repletion, darkness (low photosynthesis rate), normal state reducing cytosol or iron sufficiency in an anoxic environment like the heterocyst. Under stronger oxidative conditions caused either by iron repletion and H_2O_2, FurC:Zn-Fe repressor will be released rapidly from DNA after irreversible MCO reacting rapidly on Fe^{2+}-FurC:Zn already bound to DNA, whereas all the free FurC:Zn pool will be reversible oxidized under inactive oxidized oligomers. This dual oxidation allows a faster recovery of FurC:Zn activity and therefore a faster response to a changing environment.

Acknowledgments

Authors thank financial support from Ministerio de Ciencia, Innovación y Universidades (grant 438 PID2019-104889GB-I00), Gobierno de Aragón (grants E35_20R Biología Estructural). Authors would like to acknowledge the Proteomics Facility of Servicios Científico Técnicos (IACS-Universidad de Zaragoza). This work has been partially supported by ARCANE Labex and GRAL Labex within the framework of the CBHEUR-GS (ANR-17-EURE-0003) and the CNRS International Emerging Action- IEA2022. This work used the SEC-MALLS-RI platform of the Institute de Recherches Interdisciplinaires de Grenoble (IRIG) supported by the GRAL Labex (ANR-10-LABX-49-01).

Data availability statement

The data underlying this article are available in the article and in its online supplementary material.

References

1. Sevilla E, Bes MT, Peleato ML *et al.* Fur-like proteins: Beyond the ferric uptake regulator (Fur) paralog. *Archives of biochemistry and biophysics* 2021;**701**:108770. doi: 10.1016/j.abb.2021.108770
2. Fuangthong M, Herbig AF, Bsat N *et al.* Regulation of the *Bacillus subtilis fur* and *perR* genes by PerR: not all members of the PerR regulon are peroxide inducible. *Journal of bacteriology* 2002;**184**(12):3276-86. doi: 10.1128/jb.184.12.3276-3286.2002
3. Moore CM, Nakano MM, Wang T *et al.* Response of *Bacillus subtilis* to nitric oxide and the nitrosating agent sodium nitroprusside. *Journal of bacteriology* 2004;**186**(14):4655-64. doi: 10.1128/JB.186.14.4655-4664.2004
4. Gancz H, Merrell DS. The *Helicobacter pylori* Ferric Uptake Regulator (Fur) is essential for growth under sodium chloride stress. *J Microbiol* 2011;**49**(2):294-8. doi: 10.1007/s12275-011-0396-7
5. Sethu R, Goure E, Signor L *et al.* Reaction of PerR with Molecular Oxygen May Assist H_2O_2 Sensing in Anaerobes. *ACS chemical biology* 2016;**11**(5):1438-44. doi: 10.1021/acschembio.5b01054
6. Chen XK, Li XY, Ha YF *et al.* Ferric Uptake Regulator Provides a New Strategy for Acidophile Adaptation to Acidic Ecosystems. *Applied and environmental microbiology* 2020;**86**(11). doi: 10.1128/AEM.00268-20
7. Guio J, Sarasa-Buisan C, Velazquez-Campoy A *et al.* 2-oxoglutarate modulates the affinity of FurA for the *ntcA* promoter in *Anabaena* sp. PCC 7120. *FEBS letters* 2020;**594**(2):278-89. doi: 10.1002/1873-3468.13610
8. Fillat MF. The FUR (ferric uptake regulator) superfamily: diversity and versatility of key transcriptional regulators. *Archives of biochemistry and biophysics* 2014;**546**:41-52. doi: 10.1016/j.abb.2014.01.029
9. Perard J, Nader S, Levert M *et al.* Structural and functional studies of the metalloregulator Fur identify a promoter-binding mechanism and its role in Francisella tularensis virulence. *Communications biology* 2018;**1**:93. doi: 10.1038/s42003-018-0095-6
10. Sein-Echaluce VC, Pallares MC, Lostao A *et al.* Molecular basis for the integration of environmental signals by FurB from *Anabaena* sp. PCC 7120. *The Biochemical journal* 2018;**475**(1):151-68. doi: 10.1042/BCJ20170692
11. Yingping F, Lemeille S, Talla E *et al.* Unravelling the cross-talk between iron starvation and oxidative stress responses highlights the key role of PerR (*alr0957*) in peroxide signalling in the cyanobacterium *Nostoc* PCC 7120. *Environmental microbiology reports* 2014;**6**(5):468-75. doi: 10.1111/1758-2229.12157
12. Sevilla E, Sarasa-Buisan C, Gonzalez A *et al.* Regulation by FurC in *Anabaena* Links the Oxidative Stress Response to Photosynthetic Metabolism. *Plant & cell physiology* 2019;**60**(8):1778-89. doi: 10.1093/pcp/pcz094
13. Sarasa-Buisan C, Guio J, Broset E *et al.* FurC (PerR) from *Anabaena* sp. PCC7120: a versatile transcriptional regulator engaged in the regulatory network of heterocyst development and nitrogen fixation. *Environmental microbiology* 2021. doi: 10.1111/1462-2920.15552
14. Bsat N, Herbig A, Casillas-Martinez L *et al. Bacillus subtilis* contains multiple Fur homologues: identification of the iron uptake (Fur) and peroxide regulon (PerR)

repressors. *Molecular microbiology* 1998;**29**(1):189-98. doi: 10.1046/j.1365-2958.1998.00921.x

15. Traore DA, El Ghazouani A, Ilango S *et al.* Crystal structure of the apo-PerR-Zn protein from *Bacillus subtilis*. *Molecular microbiology* 2006;**61**(5):1211-9. doi: 10.1111/j.1365-2958.2006.05313.x
16. Lee JW, Helmann JD. The PerR transcription factor senses H_2O_2 by metal-catalysed histidine oxidation. *Nature* 2006; **440** (7082):363-7. doi: 10.1038/nature04537
17. Lee JW, Helmann JD. Biochemical characterization of the structural Zn^{2+} site in the *Bacillus subtilis* peroxide sensor PerR. *The Journal of biological chemistry* 2006;**281**(33):23567-78. doi: 10.1074/jbc.M603968200
18. Jacquamet L, Traore DA, Ferrer JL *et al.* Structural characterization of the active form of PerR: insights into the metal-induced activation of PerR and Fur proteins for DNA binding. *Molecular microbiology* 2009;**73**(1):20-31. doi: 10.1111/j.1365-2958.2009.06753.x
19. Traore DA, El Ghazouani A, Jacquamet L *et al.* Structural and functional characterization of 2-oxo-histidine in oxidized PerR protein. *Nature chemical biology* 2009;**5**(1):53-9. doi: 10.1038/nchembio.133
20. Herbig AF, Helmann JD. Roles of metal ions and hydrogen peroxide in modulating the interaction of the *Bacillus subtilis* PerR peroxide regulon repressor with operator DNA. *Molecular microbiology* 2001;**41**(4):849-59. doi: 10.1046/j.1365-2958.2001.02543.x
21. Perard J, Coves J, Castellan M *et al.* Quaternary Structure of Fur Proteins, a New Subfamily of Tetrameric Proteins. *Biochemistry* 2016;**55**(10):1503-15. doi: 10.1021/acs.biochem.5b01061
22. Jumper J, Evans R, Pritzel A *et al.* Highly accurate protein structure prediction with AlphaFold. *Nature* 2021;**596**(7873):583-9. doi: 10.1038/s41586-021-03819-2
23. Varadi M, Anyango S, Deshpande M *et al.* AlphaFold Protein Structure Database: massively expanding the structural coverage of protein-sequence space with high-accuracy models. *Nucleic acids research* 2022;**50**(D1):D439-D44. doi: 10.1093/nar/gkab1061
24. Berman HM, Westbrook J, Feng Z *et al.* The Protein Data Bank. *Nucleic acids research* 2000;**28**(1):235-42. doi: 10.1093/nar/28.1.235
25. Krissinel E, Henrick K. Inference of macromolecular assemblies from crystalline state. *Journal of molecular biology* 2007;**372**(3):774-97. doi: 10.1016/j.jmb.2007.05.022
26. D'Autreaux B, Pecqueur L, Gonzalez de Peredo A *et al.* Reversible redox- and zinc-dependent dimerization of the *Escherichia coli* fur protein. *Biochemistry* 2007;**46**(5):1329-42. doi: 10.1021/bi061636r

27 Wiseman T, Williston S, Brandts JF et al. Rapid Measurement of Binding Constants and Heats of Binding Using a New Titration Calorimeter. Anal Biochem 1989;179(1):131-7. doi: Doi 10.1016/0003-2697(89)90213-3

28 Xiao Z, Wedd AG. The challenges of determining metal–protein affinities. Natural Product Reports 2010;27(5):768-89. doi: 10.1039/b906690j

29. Sein-Echaluce VC, Gonzalez A, Napolitano M *et al.* Zur (FurB) is a key factor in the control of the oxidative stress response in *Anabaena* sp. PCC 7120.

Environmental microbiology 2015;**17**(6):2006-17. doi: 10.1111/1462-2920.12628

30. Makobongo MO, Gancz H, Carpenter BM *et al.* The oligo-acyl lysyl antimicrobial peptide C(1)(2)K-2beta(1)(2) exhibits a dual mechanism of action and demonstrates strong in vivo efficacy against *Helicobacter pylori*. *Antimicrobial agents and chemotherapy* 2012;**56**(1):378-90. doi: 10.1128/AAC.00689-11
31. Kebouchi M, Saul F, Taher R *et al.* Structure and function of the *Leptospira interrogans* peroxide stress regulator (PerR), an atypical PerR devoid of a structural metal-binding site. *The Journal of biological chemistry* 2018;**293**(2):497-509. doi: 10.1074/jbc.M117.804443
32. Dian C, Vitale S, Leonard GA *et al.* The structure of the *Helicobacter pylori* ferric uptake regulator Fur reveals three functional metal binding sites. *Molecular microbiology* 2011;**79**(5):1260-75. doi: 10.1111/j.1365-2958.2010.07517.x
33. Vitale S, Fauquant C, Lascoux D *et al.* A ZnS(4) structural zinc site in the *Helicobacter pylori* ferric uptake regulator. *Biochemistry* 2009;**48**(24):5582-91. doi: 10.1021/bi9004396
34. Ortiz de Orue Lucana D, Schrempf H. The DNA-binding characteristics of the *Streptomyces reticuli* regulator FurS depend on the redox state of its cysteine residues. *Molecular & general genetics : MGG* 2000;**264**(3):341-53. doi: 10.1007/s004380000328
35. Ortiz de Orue Lucana D, Troller M, Schrempf H. Amino acid residues involved in reversible thiol formation and zinc ion binding in the *Streptomyces reticuli* redox regulator FurS. *Molecular genetics and genomics : MGG* 2003;**268**(5):618-27. doi: 10.1007/s00438-002-0776-0
36. Tong H, Dong Y, Wang X *et al.* Redox-Regulated Adaptation of *Streptococcus oligofermentans* to Hydrogen Peroxide Stress. *mSystems* 2020;**5**(2). doi: 10.1128/mSystems.00006-20
37. Nakao M, Okamoto S, Kohara M *et al.* CyanoBase: the cyanobacteria genome database update 2010. *Nucleic acids research* 2010;**38**(Database issue):D379-D81. doi: 10.1093/nar/gkp915
38. Herrero A, Flores E. Genetic responses to carbon and nitrogen availability in *Anabaena*. *Environmental microbiology* 2019;**21**(1):1-17. doi: 10.1111/1462-2920.14370
39. Hillmann F, Fischer RJ, Saint-Prix F *et al.* PerR acts as a switch for oxygen tolerance in the strict anaerobe *Clostridium acetobutylicum*. *Molecular microbiology* 2008;**68**(4):848-60. doi: 10.1111/j.1365-2958.2008.06192.x

Figure legends

Figure 1. ClustalW alignment of PerR primary sequences. (An) *Anabaena* sp., (Bs) *Bacillus subtilis*, (Cj) *Campylobacter jejuni*, (Li) *Leptospira interrogans* and (Sp) *Streptococcus pyogenes*. Cysteine residues are shown in bold red. The cysteines that coordinate the structural Zn^{2+} ion are underlined. Residues that coordinate the regulatory metal in *B. subtilis*, *C. jejuni*, *L. interrogans*, and *S. pyogenes* PerRs are shown in blue and underlined. The 2 His oxidizable by MCO in *B. subtilis* are shown in bold. Conserved residues in FurC corresponding to the regulatory metal binding site in BsPerR are shown in blue. The N and D residues proposed in this work as substitutes in FurC from *Anabaena* sp. for the BsPerR Asp85 are shown in bold.

Figure 2. Analysis of oligomerization of FurC:Zn as purified. (A) SEC elution profiles of different aliquots of purified FurC:Zn (50 mM Tris-HCl, 150 mM NaCl pH 7.5) incubated without any additive (green), with 2 mM DTT for 15 min (red) and with NaCl 0.5 M for 30 min followed with 2 mM DTT for 10 min (blue) prior to separation. The Superdex S200 Increase 10/30 column was equilibrated in 50 mM Tris-HCl, 150 mM NaCl, 10% glycerol pH 7.5; **(B)** 17% non-reducing SDS-PAGE gel stained with Coomassie blue of FurC:Zn as purified with and without DTT. The gel shows the presence of disulfide bonds in FurC:Zn without any treatment and its reduction after pre-incubation of FurC:Zn with 10 mM DTT. **(C)** Simplified scheme of the different major states of FurC:Zn in solution (left panel) and in the SDS-PAGE gel without and with DTT (right panel). According to SEC-MALLS-RI, the most abundant covalent species bridging two subunits present in the gel are different to the functional FurC:Zn dimers and are formed by bridged FurC subunits which belonged to different dimers in the tetramer. Higher oligomeric forms as well as other potential intermolecular disulfide bridges have been omitted for clarity. **(D)** and **(E)** Molecular weight determination by SEC-MALLS-RI of the fractions “peak 1” and “peak 2” collected from SEC described in (A): peak 1 **(D)** and peak 2 **(E)**. The black traces correspond to the calculated Log Molar mass values.

Figure 3. Reversible oligomerization of FurC:Zn dimer. (A) SEC elution profiles of different aliquots of FurC:Zn at 2 $mg.mL^{-1}$ (122 µM) in 50 mM Tris-HCl, 150 mM NaCl pH 7.5, incubated prior to separation: without any additive (black), with 5 mM diamide for

30 min (solid blue line); with 5 mM H_2O_2 for 30 min (solid red line); with 5 mM diamide for 30min followed by addition of 10 mM DTT for 10 min (dashed blue line); or with 5 mM H_2O_2 for 30 min followed by addition of 10 mM DTT for 10 min (dashed red line). The Superdex S200 Increase 10/30 column was equilibrated in 50 mM Tris-HCl, 150 mM NaCl pH 7.5 and performed at 0.5 $mL.min^{-1}$. **(B)** non-reducing SDS-PAGE gel (4-20% Biorad) stained with Coomassie blue of FurC:Zn samples presented in (A) prior injection on SEC. **(C)** Molar mass determination by SEC-MALLS-RI of the eluted fraction of the H_20_2 treated FurC:Zn sample showing the presence of well-defined oligomers. The UV at 280 nm profile was shown together with the gray traces corresponding to the calculated Log Molar mass values.

Figure 4. EMSA analyses of the interaction between FurC:Zn and the promoter region of the *prxA* gene in the presence of Mn^{2+} or Zn^{2+}. As non-specific DNA control, the internal region of the *pkn22* gene was used. Free DNA or DNA incubated with 0.2 µM of FurC:Zn without added divalent metal ions or in the presence of 5, 50, 100 µM of the indicated divalent metal ion were tested. Mixtures were incubated in the reaction buffer containing 10 mM Bis-Tris pH 7.5, 40 mM KCl, 1 mM DTT, 5% glycerol and 0.05 mg/mL bovine serum albumin before being loaded on native 6% polyacrylamide gels.

Figure 5. MALDI-TOF-MS profiles of FurC:Zn under different incubation conditions show that FurC:Zn is oxidized by MCO in the presence of Fe^{2+}. Prior to the determination of molecular mass, 40 µM of FurC:Zn were treated with freshly prepared 40 µM of $MnCl_2$ or 40 µM of $FeSO_4$ during 30 min under aerobic conditions. Afterwards the samples were treated with or without 100 µM of H_2O_2 and dialyzed against Tris-HCl 50 mM pH 7.5, NaCl 150 mM. (a) FurC:Zn without treatment (b) FurC:Zn incubated with Fe^{2+} (c) FurC:Zn incubated with Fe^{2+} and H_2O_2, (d) FurC:Zn incubated with Mn^{2+} and H_2O_2.

Figure 6. **DNA-binding activity of FurC:Zn under different oxidation regimes determined by EMSA.** Assays were carried out with 200 nM FurC:Zn under different incubation conditions using the *prxA* promoter as a specific FurC:Zn target and an internal region of the *pkn22* gene as competitor, unspecific DNA. Prior to the assay, 40 µM FurC:Zn was pre-reduced with 10 mM DTT. Afterwards, DTT was removed from the

fraction by buffer exchange with a centrifugal filter unit. After reduction, 20 μM of FurC:Zn was pretreated aerobically either with or without 20 μM of Fe^{2+} (lanes 5 and 6). Lane 1 contains free DNA, lanes 2-6 contain DNA fragments with the different preincubated FurC:Zn fractions (2) pre-reduced FurC:Zn, (3) pre-reduced FurC:Zn treated with 5 mM H_2O_2, (5) FurC:Zn treated with 5 mM H_2O_2 and then with 10 mM DTT, (6) FurC:Zn incubated with Fe^{2+}, (7) FurC:Zn incubated with Fe^{2+} and treated with 10 mM DTT. The incubated proteins were mixed with the DNA promoter in a reaction buffer containing 10 mM Bis-Tris pH 7.5, 40 mM KCl, 100 μM $MnCl_2$, 5% glycerol and 0.05 mg/mL bovine serum albumin before being loaded on native 6% polyacrylamide gels.

Figure 7. **AlphaFold FurC predictions.** The models are colored according to the per-residue confidence metric (pLDDT). **(A)** Model for the structure of the FurC dimer showing the loop containing C86. **(B)** Plots showing LDDT prediction and **(C)** Predicted Aligned Error of the FurC dimer. **(D)** Model for the structure of the FurC tetramer. **(E)** and **(F)** Plots showing predicted LDDT and Predicted Aligned Error of the FurC tetramer, respectively.

Figure 8. Comparison between the structures of FurC dimers obtained with AlphaFold colab and SWISSMODEL. MnBsPerR was used as template for building the SWISSMODEL structures. **(A)** Superposition of AlphaFold (grey) and SWISS-MODEL (blue) structures of dimeric FurC. **(B)** Metal-binding sites in AlphaFold (grey) and SWISS-MODEL (blue) models. **(C)** Metal-binding sites in the SWISS-MODEL built using MnBsPerR as template shown in blue and in the resolved structure (PDB 3F8N) represented in pink.

Figure 9. Predicted distances among Cα of Cys86 residues in a FurC tetramer modelled with AlphaFold v2. Two different orientations of the modelled tetramer are displayed. Bonds between Cys86 residues from monomer to monomer in a dimeric unit are represented with dashes in red and blue whereas interdimer distances are shown in grey. A zoom view of the tetramer displayed in the right orientation shows distances in angstroms.

Figure 10. Integrative model of the two levels of FurC oxidation. (A) Reversible intermolecular disulfide bridge formation between FurC dimers under mild oxidant conditions or iron deficiency. **(B)** Under stronger oxidative conditions caused either by iron repletion and O_2 or Fe^{+2} and H_2O_2, irreversible metal catalyzed oxidation of FurC is produced.

Figure 1:

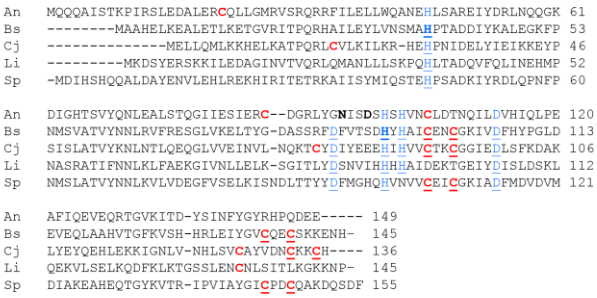
An MQQQAISTKPIRSLEDALERCQLLGMRVSRQRRFILELLWQANEHLSAREIYDRLNQQGK 61
Bs --------MAAHELKEALETLKETGVRITPQRHAILEYLVNSMAHPTADDIYKALEGKFP 53
Cj ----------MELLQMLKKHELKATPQRLCVLKILKR-HEHPNIDELYIEIKKEYP 46
Li ---------MKDSYERSKKILEDAGINVTVQRLQMANLLLSKPQHLTADQVFQLINEHMP 52
Sp -MDIHSHQQALDAYENVLEHLREKHIRITETRKAIISYMIQSTEHPSADKIYRDLQPNFP 60
An DIGHTSVYQNLEALSTQGIIESIERC--DGRLYGNISDSHSHVNCLDTNQILDVHIQLPE 120
Bs NMSVATVYNNLRVFRESGLVKELTYG-DASSRFDFVTSDHYHAICENCGKIVDFHYPGLD 113
Cj SISLATVYKNLNTLQEQGLVVEINVL-NQKTCYDIYEEEHIHVVCTKCGGIEDLSFKDAK 106
Li NASRATIFNNLKLFAEKGIVNLLELK-SGITLYDSNVIHHHHAIDEKTGEIYDISLDSKL 112
Sp NMSLATVYNNLKVLVDEGFVSELKISNDLTTYYDFMGHQHVNVVCEICGKIADFMDVDVM 121
An AFIQEVEQRTGVKITD-YSINFYGYRHPQDEE----- 149
Bs EVEQLAAHVTGFKVSH-HRLEIYGVCQECSKKENH- 145
Cj LYEYQEHLEKKIGNLV-NHLSVCAYVDNCKKCH---- 136
Li QEKVLSELKQDFKLKTGSSLENCNLSITLKGKKNP- 145
Sp DIAKEAHEQTGYKVTR-IPVIAYGICPDCQAKDQSDF 155

Figure 2

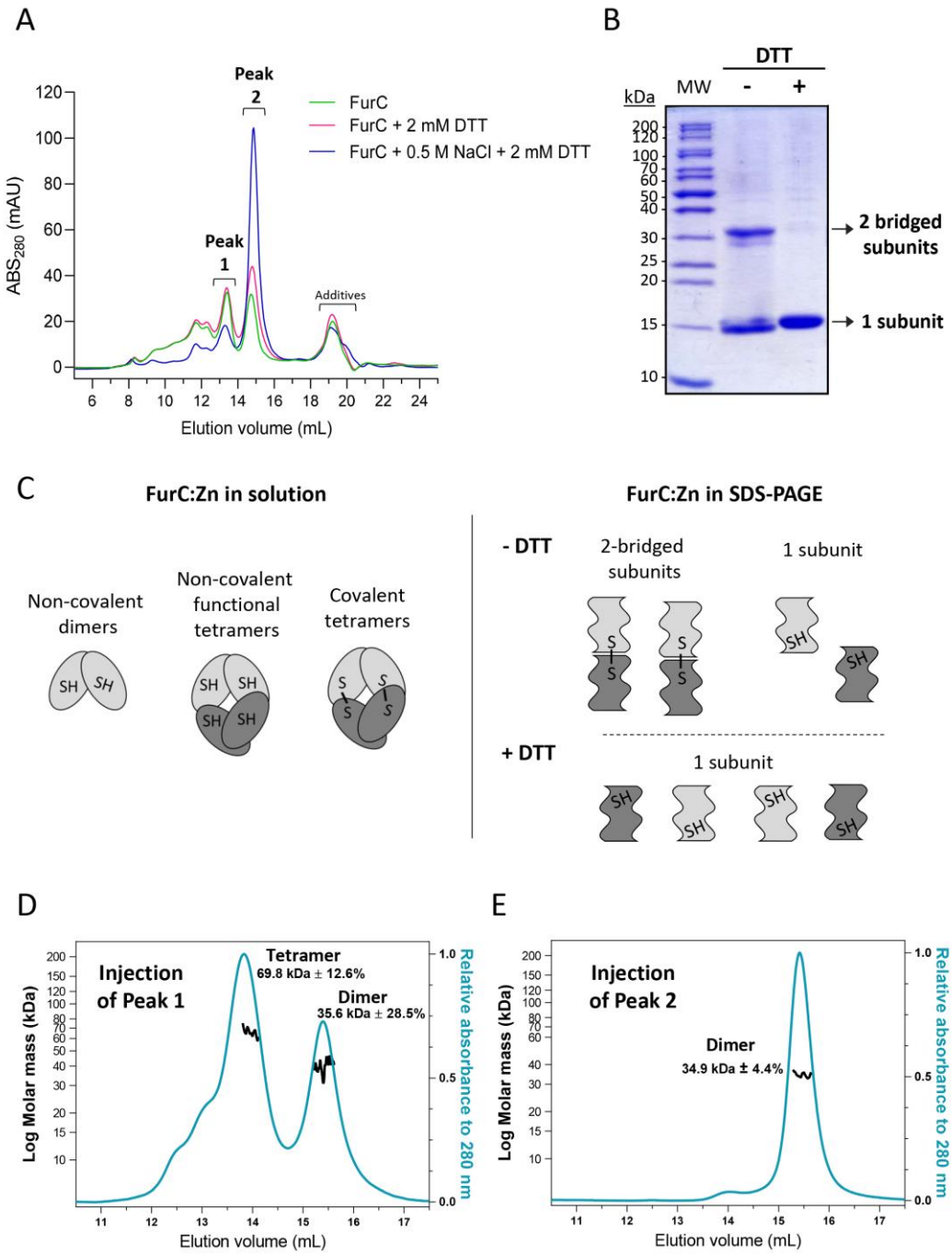
A
Peak 2
Peak 1
Additives
FurC
FurC + 2 mM DTT
FurC + 0.5 M NaCl + 2 mM DTT
ABS280 (mAU)
Elution volume (mL)
B
DTT
MW
kDa
2 bridged subunits
1 subunit
C
FurC:Zn in solution
Non-covalent dimers
Non-covalent functional tetramers
Covalent tetramers
FurC:Zn in SDS-PAGE
- DTT
2-bridged subunits
1 subunit
+ DTT
1 subunit
D
Injection of Peak 1
Tetramer
69.8 kDa ± 12.6%
Dimer
35.6 kDa ± 28.5%
Log Molar mass (kDa)
Relative absorbance to 280 nm
Elution volume (mL)
E
Injection of Peak 2
Dimer
34.9 kDa ± 4.4%
Log Molar mass (kDa)
Relative absorbance to 280 nm
Elution volume (mL)

Figure 3

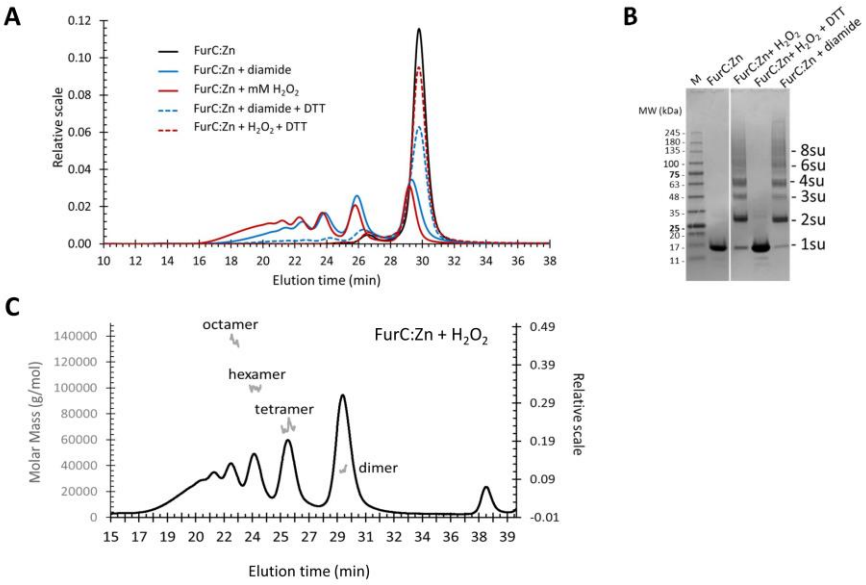

Figure 4

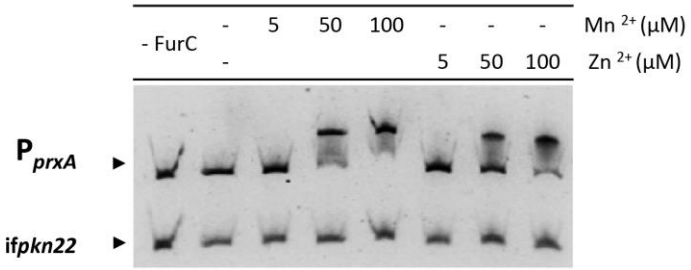

Figure 5

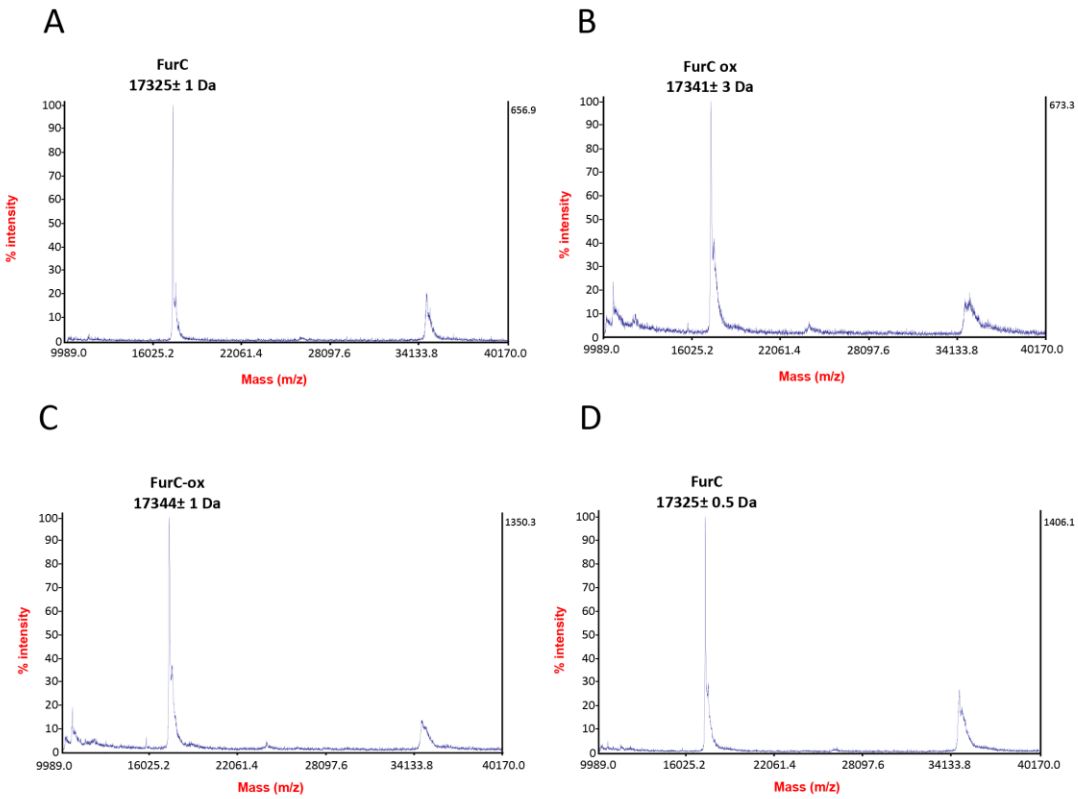
A
FurC
17325± 1 Da
656.9
% intensity
Mass (m/z)
B
FurC ox
17341± 3 Da
673.3
% intensity
Mass (m/z)
C
FurC-ox
17344± 1 Da
1350.3
% intensity
Mass (m/z)
D
FurC
17325± 0.5 Da
1406.1
% intensity
Mass (m/z)
9989.0
16025.2
22061.4
28097.6
34133.8
40170.0

Figure 6

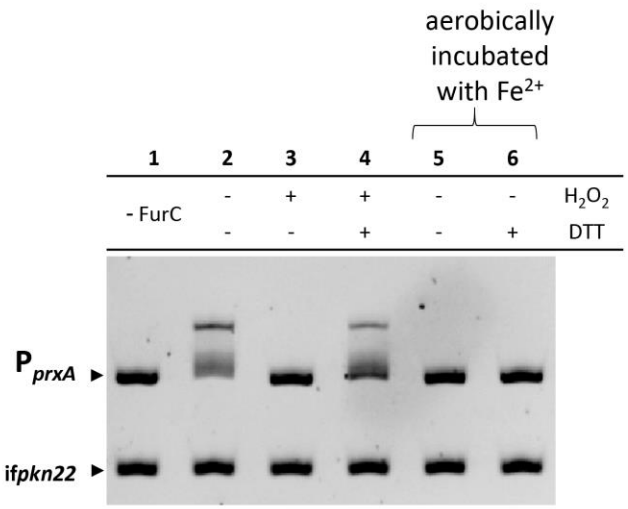
aerobically
incubated
with Fe2+
1
2
3
4
5
6
- FurC
-
+
+
-
-
H2O2
-
-
+
-
+
DTT
PprxA
ifpkn22

Figure 7

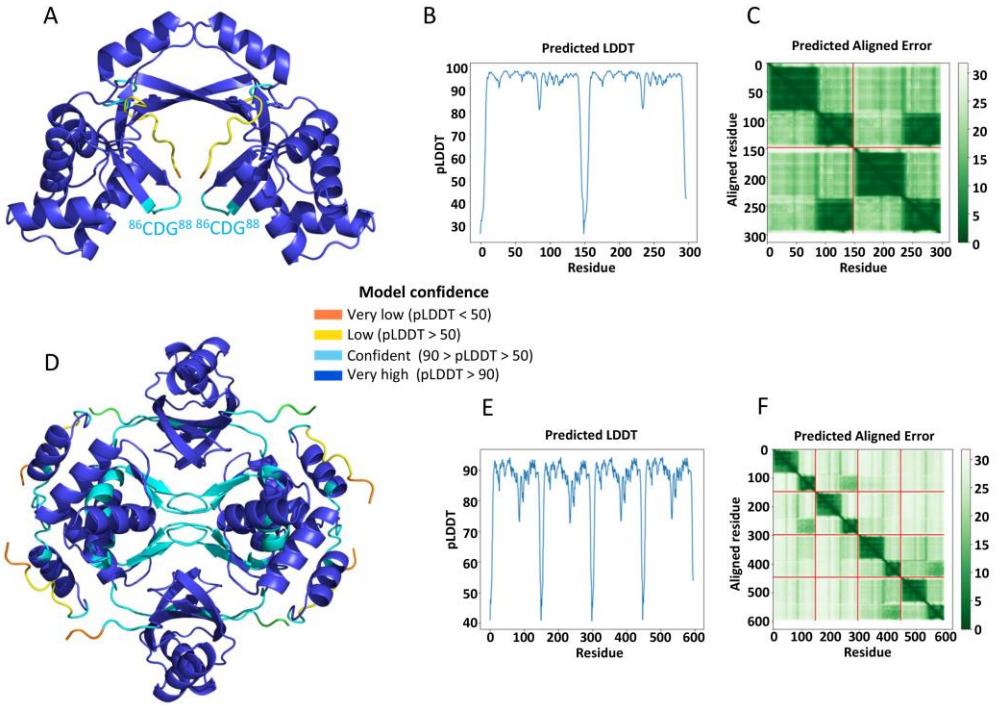

Figure 8

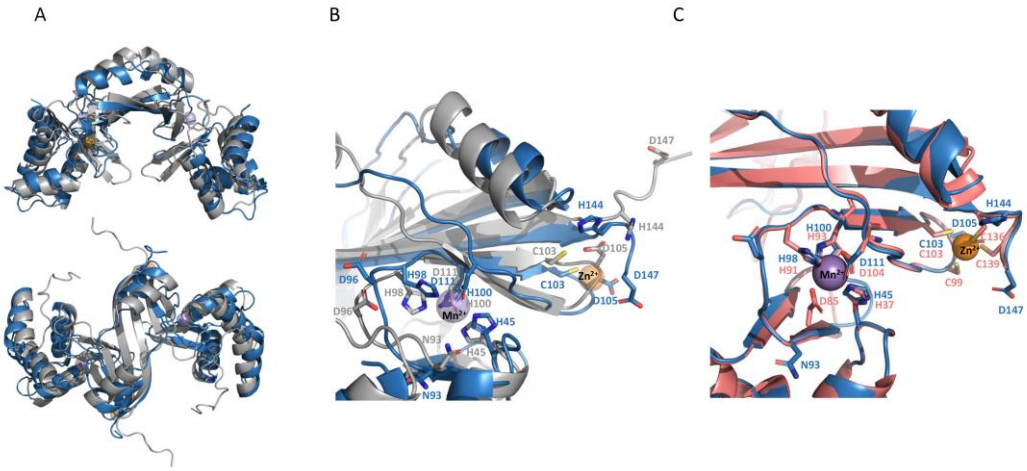

Figure 9

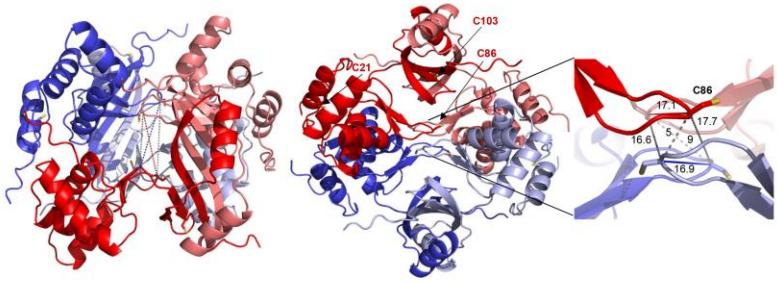

Figure 10

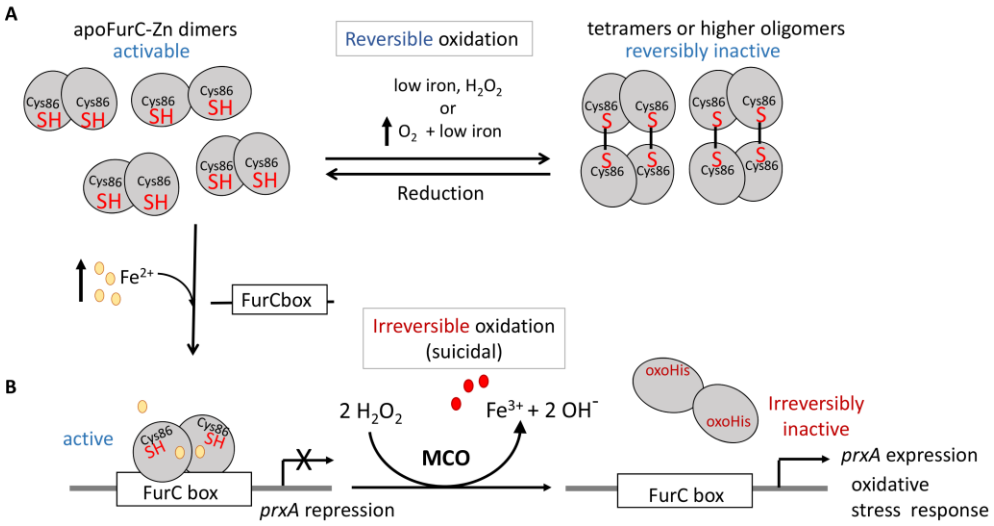

Supporting Information

Metal binding and oligomerization properties of FurC (PerR) from *Anabaena* sp. PCC7120: an additional layer of regulation?

Cristina Sarasa-Buisan[1], Etienne Emonot[2], Marta Martínez-Júlvez[1], Emma Sevilla[1], Adrián Velázquez-Campoy[1], Serge Crouzy[2] (*in memoriam*), M. Teresa Bes[1], Isabelle Michaud-Soret[2*&] and María F. Fillat[1*&].

[1] Departamento de Bioquímica y Biología Molecular y Celular e Instituto de Biocomputación y Física de Sistemas Complejos (Bifi). Universidad de Zaragoza. 50009-Zaragoza, Spain.

[2] Université Grenoble Alpes, CNRS CEA, IRIG-LCBM 38000 Grenoble, France.

*Both authors contributed equally to this work

[&] Corresponding authors:

MF Fillat fillat@unizar.es

I Michaud-Soret isabelle.michaud-soret@cea.fr

Table S1. Metal content analysis by ICP-OES. Results are reported as two independent measurements separated by a comma and the corresponding average is shown in bold.

Protein (purification)	Molar ratio of Zn to FurC subunit	Molar ratio of Fe to FurC subunit
FurC (DEAE + heparin)	1.138, 1.131 **1.135**	0.340, 0.440 **0.390**
FurC (Heparin + DEAE)	0.737, 0.930 **0.834**	0.179, 0.447 **0.313**
FurC dimer (Heparin + DEAE + SEC)	1.192, 1.337 **1.265**	0.426, 0.730 **0.578**

Table S2. Parameters estimated by ITC for the interaction of FurC:Zn with Mn^{2+} and FurC:Zn with Zn^{2+}. Limiting values for the apparent affinity constants (K_d)*, enthalpies of the interactions (ΔH) and stoichiometries (n) are shown.

Sample	K_d (nM)*	ΔH (kcal/mol)	n
FurC:Zn vs Mn^{2+}	< 100	-23.6	1.1
FurC:Zn vs Mn^{2+} (+DTT)	< 100	-25.4	0.96
FurC:Zn vs Mn^{2+} (+TCEP)	< 100	-30.8	0.83
FurC:Zn vs Mn^{2+} (+ H_2O_2)	< 100	-28.2	0.86
FurC:Zn vs Zn^{2+}	< 100	-16.6	1.2
FurC:Zn vs Zn^{2+} (+DTT)	< 100	17.4	1.2
FurC:Zn vs Zn^{2+} (+TCEP)	< 100	-20.0	1.0
FurC:Zn vs Zn^{2+} (+ H_2O_2)	< 100	-17.2	1.0

* Please, note that under these conditions the apparent dissociation constants do not permit reliable quantitation of binding affinity (refs 27 and 28 in main text). Similar experimental conditions to these used in EMSA tests were chosen in order to support the results on the effect of Mn^{2+} and Zn^{2+} in FurC:Zn DNA-binding .

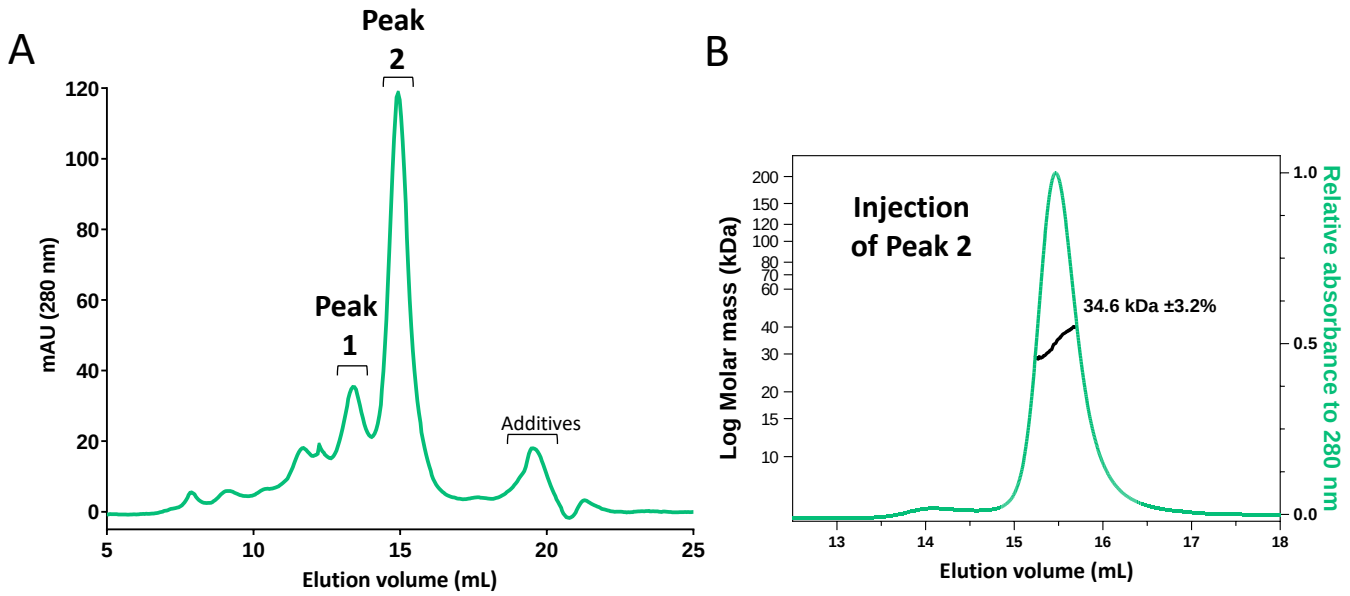

Figure S1. SEC chromatography and molecular weight determination by SEC-MALLS-RI of purified FurC:Zn in presence of TCEP in the columns along the whole process. **(A)** Purified FurC:Zn in 50 mM Tris-HCl, 150 mM NaCl pH 7.5 was incubated with NaCl 0.5 M for 30 min and with 2 mM DTT for 15 min. The Superdex S200 Increase 10/30 column was equilibrated in 50 mM Tris-HCl, 150 mM NaCl pH 7.5, 0.5 mM TCEP. **(B)** Molecular weight determination by SEC-MALLS-RI of the major peak isolated from SEC (see panel A) using the same equilibration buffer as in SEC chromatography.

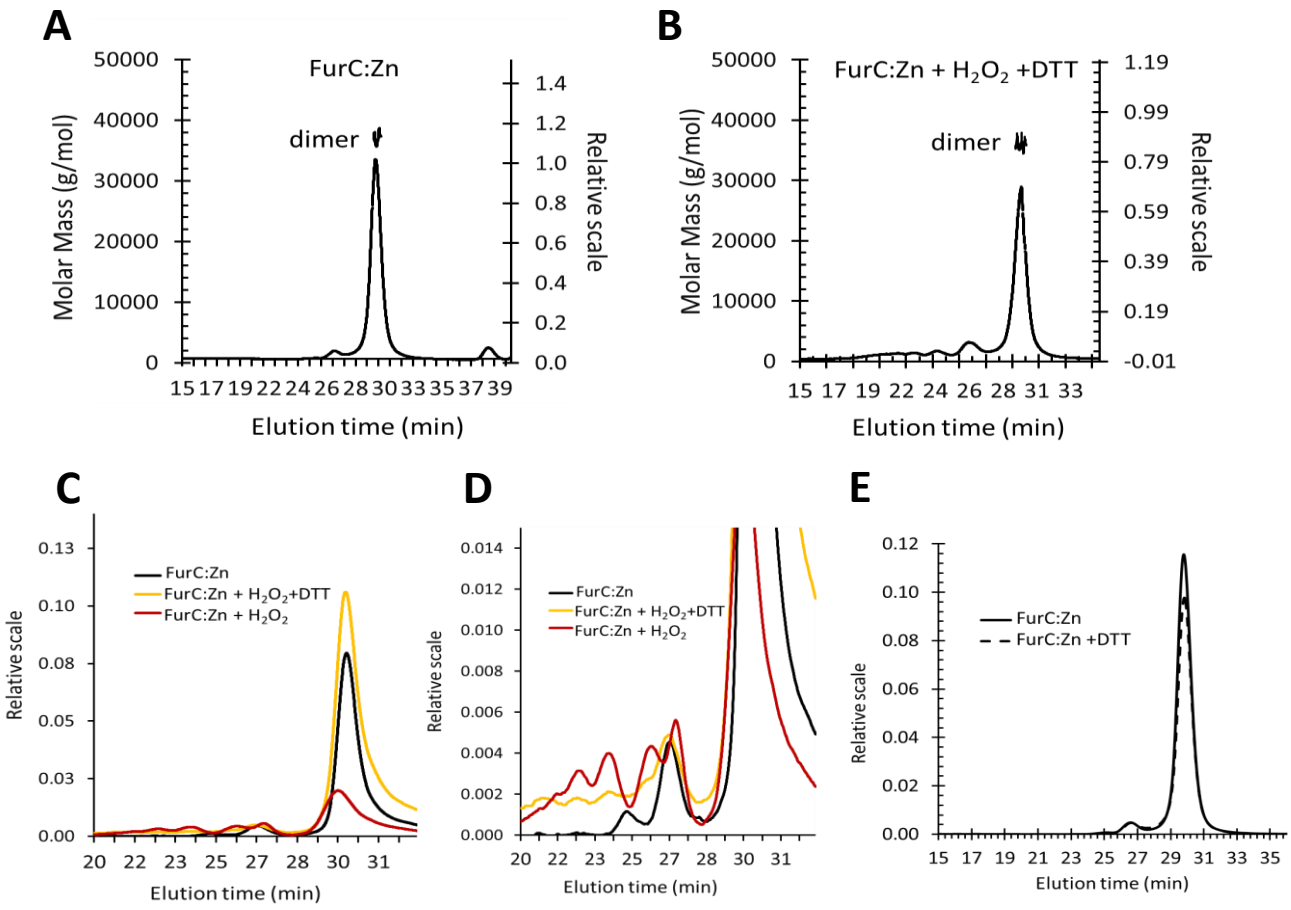

Figure S2. Reversible oligomerization of FurC:Zn dimer upon oxidation and reduction.

Molecular mass determination by SEC-MALLS-RI of the eluted fraction FurC:Zn dimer **(A)** and FurC:Zn treated with 5 mM H_2O_2 for 30 min followed by addition of 10 mM DTT for 10 min **(B)** as described in Figure 3. **(C)** SEC elution profiles of different aliquots of FurC:Zn at 20 µM in 50 mM Tris-HCl, 150 mM NaCl pH 7.5, incubated prior to separation: without any additive (black), with 5 mM H_2O_2 for 30 min (red); with 5 mM H_2O_2 for 30 min followed by addition of 10 mM DTT for 10 min (orange). The Superdex S200 Increase 10/30 column was equilibrated in 50 mM Tris-HCl, 150 mM NaCl pH 7.5 and performed at 0.5 mL.min^{-1}. **(D)** same as in (C) with enlarged scale. **(E)** comparison of FurC:Zn and FurC:Zn treated with 10 mM DTT for 10min.

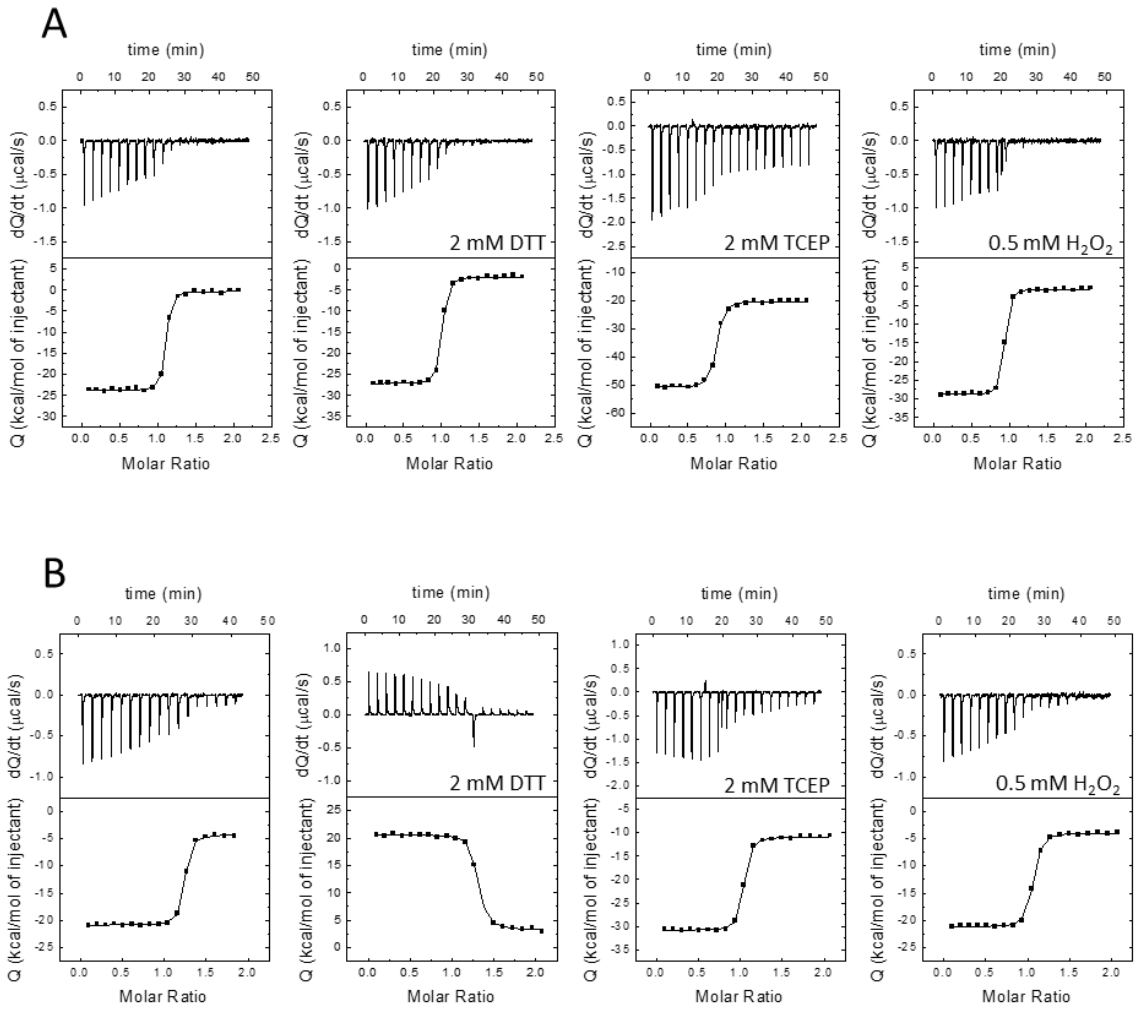

Figure S3. ITC analysis of the interaction of FurC:Zn with Mn^{2+} (A) and Zn^{2+} (B) under different redox conditions. (A) From left to right: Interaction of FurC:Zn with Mn^{2+} in the absence of reductants, in the presence of 2 mM DTT, in the presence of 2 mM TCEP and in the presence of 0.5 mM H_2O_2. **(B)** From left to right: Interaction FurC:Zn with Zn^{2+} in the absence of reducing agents, in the presence of 2 mM DTT, in the presence of 2 mM TCEP and in the presence of 500 µM H_2O_2. Figures show the thermograms (thermal power as a function of time) in the upper panels, and the binding isotherms (normalized heat as a function of the ligand/protein molar ratio) in the lower panels. FurC:Zn is at 20 µM in 50 mM Tris pH 7.5, 150 mM NaCl.

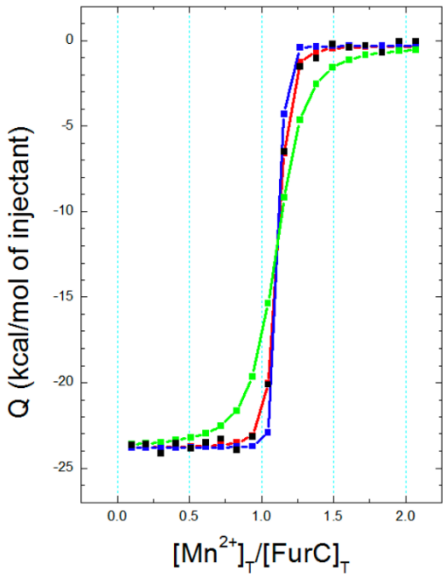

Figure S4. Simulation of binding isotherms for different values of the K_d for the interaction of FurC with Mn^{2+} (Kd ≈ 0.016 µM). The experimental data are shown as black squares and the best fit is shown as a red curve. Two simulations with 10 x K_d and 0.1 x K_d are shown as a green curve and as a blue curve, respectively. According to the best fit, the K_d is 0.016 ± 0.002 µM. In agreement with the rule-of-thumb relationship between K_d and total protein concentration for an estimation of dissociation constants ($1 < [P]_T/K_d < 1000$) [27], using 20 µM FurC:Zn, the lowest value for K_d that could be reliably estimated would be around 20 nM, indicating that our experimental data are just below the lower limit for practical determination of dissociation constants by ITC.

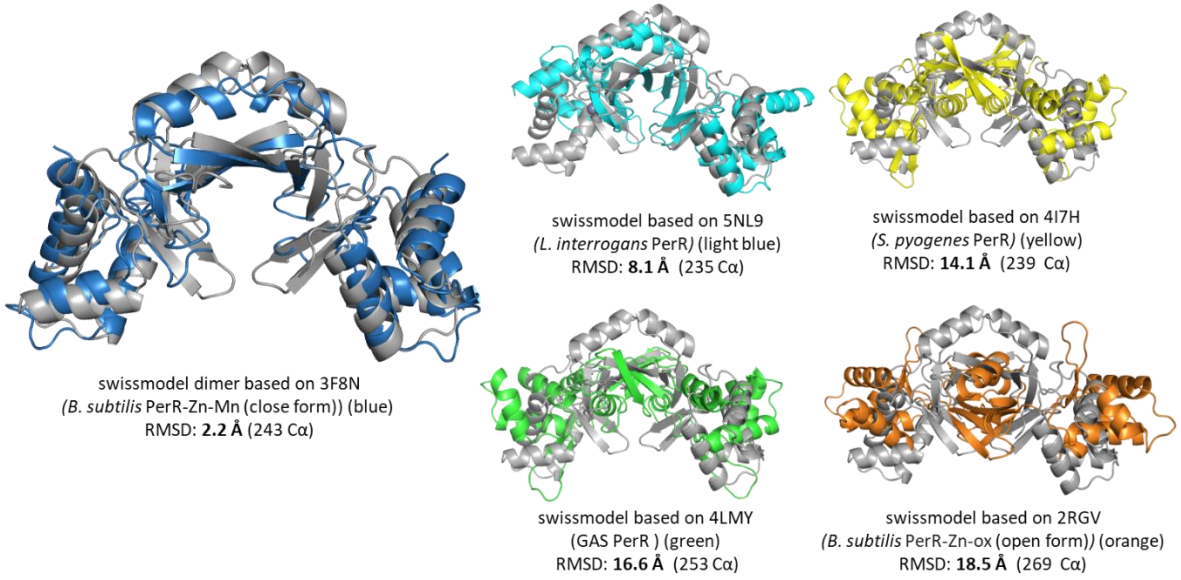

Figure S5. Comparison of the superpositions of the FurC model obtained using different approaches. The model of the *Anabaena* FurC dimer obtained using AlphaFold represented in grey was superposed with the different *Anabaena* FurC dimers built with SWISS-MODEL using several PerR proteins as templates as indicated.

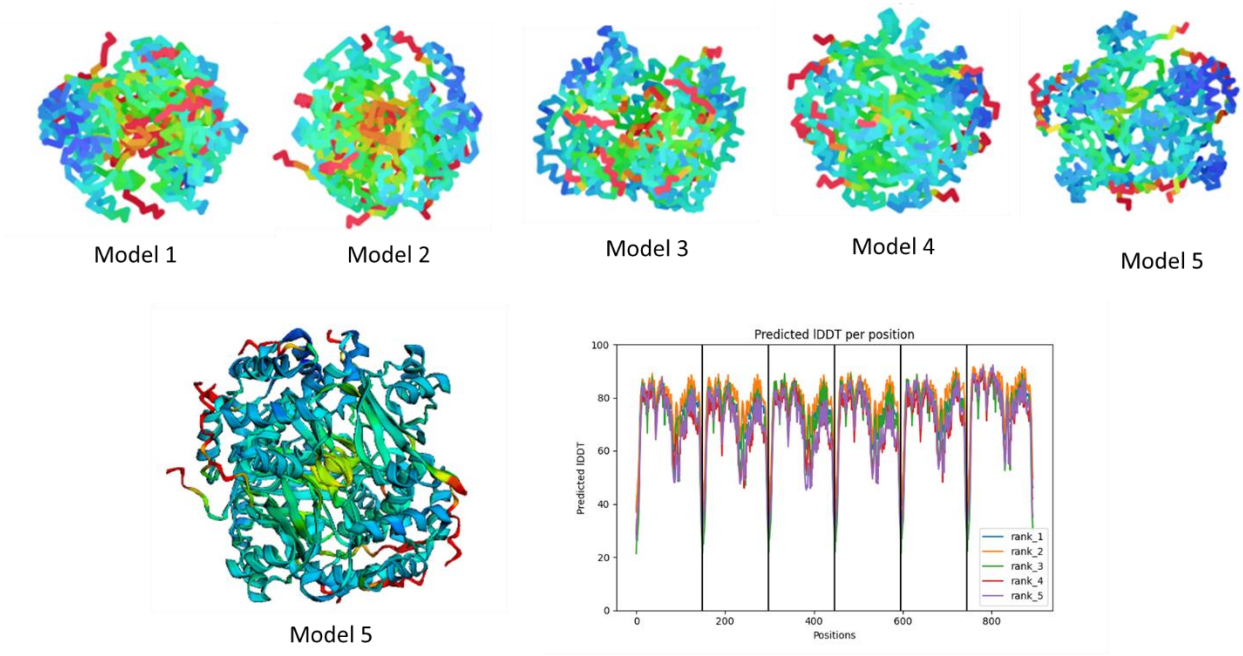

Figure S6. FurC hexamer models generated by AlphaFold v2. The color code to the per-residue confidence metric (pLDDT) and the graphs of predicted LDDT per positions show that model 5 was predicted with the highest confidence scores.

Figure S7. ClustalW alignment of FurC orthologs from several nitrogen-fixing cyanobacteria (in bold) and non-diazotrophic cyanobacteria. The conserved Cys86 in nitrogen-fixing cyanobacteria are surrounded with a red rectangle.